Original Research Article

Structural Health Monitoring
1–22

DOI: 10.1177/14759217261416108
journals.sagepub.com/home/shm

Adaptive feature mode decomposition for fault diagnosis of rotating machinery

Yuan Zhou[1], Jianchun Guo[1], Yi Liu[1] and Jiawei Xiang[1,2,3]

Abstract

In industrial scenarios, decomposition methods play a pivotal role in extracting fault information from intense background noise, which is essential for mitigating operational downtime risks. However, the performance of such decomposition methods is highly dependent on critical parameters, and inappropriate parameter tuning can significantly degrade diagnostic accuracy in practical applications. Feature mode decomposition (FMD) is widely used in fault diagnosis due to its adaptive decomposition capability; nevertheless, the unreasonable parameters setting in FMD method, lead to a wrong decomposition result. This article introduces an innovative adaptive FMD fault diagnosis approach, designed to eliminate the need for manual parameter tuning. By leveraging spectral difference preprocessing and precise parameter estimation, the method effectively achieves fault feature extraction. Simulation and experimental validation results demonstrate that the method outperforms up-to-date decomposition methods in terms of noise suppression and fault feature extraction. This adaptive FMD approach provides a robust solution for mechanical health monitoring in complex industrial environments, contributing to improved operational reliability and reduced maintenance costs.

Keywords

Feature mode decomposition, spectrum subtraction, health signals, parameter estimation, Fault diagnosis

Introduction

Rolling bearings play a critical role in the operation of rotating machinery, often enduring harsh working conditions such as high temperatures and substantial loads.[1] The operational status of these bearings is integral to the overall performance and reliability of rotating machinery.[2] Furthermore, rolling bearings are susceptible to defects caused by operational stresses and manufacturing imperfections, leading to increase vibration, noise, and even catastrophic system failures. Hence, efficient fault diagnosis methods could avert catastrophic accidents and ensure the continuous and efficient operation of rotating machinery.[3–5]

Nonstationary signal has the statistical characteristics with time and dynamic changes of instantaneous frequency and amplitude. In addition, these signals are often interfered with by strong noise, which complicates the fault feature extractions. This makes it significantly more difficult to effectively analyze and process nonstationary signals, requiring advanced signal processing techniques.[6–8] Common techniques for signal mode decomposition include wavelet transform (WT), wavelet packet transform (WPT), singular value decomposition (SVD), empirical mode decomposition (EMD), and variational mode decomposition (VMD).[9–12] WT and WPT are applied as band-pass filter banks, where mixed signals are decomposed into several narrow frequency bands, while SVD is used to separate signals into multiple modes with properties comparable to WT.[13–16] VMD is formulated as a variational optimization problem, and Wiener filters are employed to isolate modes with distinct center frequencies. Although VMD is considered effective for many

[1]College of Mechanical and Electrical Engineering, Wenzhou University, Wenzhou, China
[2]Wenzhou Key Laboratory of Advanced Equipment Dynamics and Intelligent Diagnosis-Maintenance, Wenzhou, China
[3]Pingyang Institute of Intelligent Manufacturing, Wenzhou University, Wenzhou, China

Corresponding authors:
Yi Liu, College of Mechanical and Electrical Engineering, Wenzhou University, Wenzhou 325035, China.
Email: 20230224@wzu.edu.cn

Jiawei Xiang, College of Mechanical and Electrical Engineering, Wenzhou University, Wenzhou 325035, China.
Email: jwxiang@wzu.edu.cn

applications, its performance is affected by the sensitivity of parameter selection, such as mode number and balance factors. Recently, more adaptive approaches have been introduced.[17–20] The symplectic geometric mode decomposition (SGMD) shows excellent performance in suppressing mode mixing and enabling adaptive decomposition but may introduce signal redundancy, which can limit its efficiency.[21,22] To leverage the advantages of existing methods while overcoming their limitations, Miao developed a novel signal processing approach known as feature mode decomposition (FMD).[23] FMD is leveraged adaptive finite impulse response (FIR) filters, with the filter coefficients adjusted to approximate the inverse convolution objective function of the filtered signals. Using correlation kurtosis (CK) as the target metric, the filter array refines itself to estimate the fault cycle duration. This approach ensures more thorough component separation compared to VMD.

However, the relevant parameters of FMD (filter length L, initial number of filter bands K, and final number of modes n) need to be preset, which limits its flexibility.[23] Subsequently, the particle swarm optimization algorithm is applied by Yan and colleagues[24,25] to determine the FMD parameters L and n for fault diagnosis. The scale space method was employed by Li and colleagues[26,27] to scale-transform the signal, enabling the determination of L and K for FMD, and fault features are ultimately extracted based on empirical modes to diagnose faults in shipboard antenna machinery. Combining the principle of WPT, Li et al.[28] propose a method of FMD packet (FMDP) and FMDPgram, which simplifies hyperparameter optimization into single-parameter optimization to solve the problem of FMD being limited by predefined parameters. The autoregressive model is introduced by He et al.[29] for preprocessing to reduce periodic harmonic disturbances. In FMD, the parameter L is calculated using the weighted squared envelope harmonic-to-noise ratio. An adaptive FIR filter bank is then developed, employing a 50% overlapping frequency band division method initiated with a Hanning window, to encompass the entire frequency spectrum of the fault signal and support the decomposition process. This method is demonstrated to have significant advantages in multifault feature extraction. Notably, the field of industrial fault diagnosis is currently witnessing a paradigm shift driven by emerging technologies at the intersection of machine learning and signal processing. For example, adaptive Kriging-assisted multifidelity subset simulation has advanced reliability analysis by efficiently balancing computational cost and prediction accuracy in complex systems[30]; reusable AI-enabled defect detection systems for railways, built on ensembled convolutional neural networks, have achieved robust cross-scenario generalization through transfer learning[31]; and digital twin methodologies, integrating vibration monitoring with gear wear prediction, have enabled real-time, lifecycle-oriented health management of rotating machinery.[32] These advancements collectively emphasize the growing demand for adaptive, data-driven, and cross-modal diagnostic frameworks capabilities that are yet to be fully integrated into existing signal decomposition methods like FMD. Nevertheless, the critical limitation of FMD persists: the number of decomposition modes still requires manual presetting, which limits flexibility too many modes cause redundancy, while too few lead to loss of critical fault information. This rigidity makes it difficult for FMD to align with the adaptive, data-driven trends highlighted above. In many practical applications, acquired signals are affected by significant noise,[33–36] which obscures fault features and hinders diagnosis.[37–39] Notably, health signals are often ignored in existing methods and can serve as a critical reference to mitigate noise. For example, Guo et al.[34] leveraged health signals in a convex optimization model to extract optimal fault frequency bands. However, current FMD-based methods rarely integrate health signals into parameter optimization, limiting their anti-interference capability in strong noise environments.

Despite these efforts and explorations into FMD parameter optimization and application scenarios, significant research gaps remain. First, most existing FMD parameter determination methods rely on empirical presets or single optimization objectives, failing to fully incorporate equipment health status information limiting adaptability in strong noise environments. Next, current FMD improvement methods rarely integrate with emerging intelligent diagnostic trends in industrial fields, resulting in insufficient diagnostic accuracy under multifault concurrent and dynamic working conditions. Furthermore, for the adaptive adjustment of the number of FMD decomposition modes, a universal strategy balancing information integrity and nonredundancy has not yet been formed, restricting its promotion in fault diagnosis of complex rotating machinery. To address these limitations, this article presents a novel adaptive FMD detection method aimed at enhancing FMD's resistance to signal interference and expanding its scope of application. The main contribution of this article is

(1) Spectral subtraction is introduced. It can better retain the fault information and weaken noise interference. In comparison to traditional denoising methods, stronger adaptability and robustness are exhibited, significantly enhancing fault diagnosis accuracy.

(2) A new parameter estimation method is proposed. The relationship between health and fault signals is fully utilized to select the component most rich in fault information for fault diagnosis.
(3) The FMD parameters are determined adaptively, eliminating the need for manual intervention and greatly enhancing the method's applicability.
(4) An innovative adaptive FMD method is developed to enhance both the interference resistance and robustness of FMD.

The layout of this article is structured as follows: Section "Method" provides a detailed explanation of the algorithms involved. In section "Simulation analysis," simulated signals are employed to demonstrate the validity and advantages of the proposed method. The algorithms will be validated in section "Experimental case study" using different experimental data and real engineering cases. The conclusions drawn from this study are presented in section "Conclusion."

Method

Feature mode decomposition

FMD is a nonrecursive decomposition technique whose primary objective is to effectively classify the initial signal into separate fault modes through the development of a flexible FIR filter bank.[23,24]

The core idea of FMD is to iteratively update the filter coefficients in such a way that the filtered signal can infinitely approximate the so-called "inverse convolutional objective function." Consequently, the FMD mode decomposition algorithm can be viewed as a solution to the constrained optimization problem, represented as follows:

$$\arg\max_{\{f_i(l)\}} \left\{ CK_Q(u_i) = \frac{\sum_{r=1}^{R} \left(\prod_{q=0}^{Q} u_i(r - qT_s) \right)^2}{\left(\sum_{r=1}^{R} u_i(r)^2 \right)^{Q+1}} \right\} \quad (1)$$

$$s.t. u_k(n) = \sum_{l=1}^{L} f_k(l) x(n - l + 1) \quad (2)$$

The CK is selected as the fitness function to evaluate the signal's impulsiveness and cyclic characteristics. In this setting, $u_i(n)$ represents the ith fault mode decomposition and $f_i(l)$ denotes the ith FIR filter of length L that maximizes the CK. Here, the displacement index is denoted by Q, whereas T_s represents the cycle duration of the input signal.

To solve this problem, Equation (1) can be resolved using the iterative eigenvalue decomposition algorithm. First, the decomposition mode is reformulated into a matrix representation:

$$u_i = \begin{bmatrix} u_i(1) \\ \cdots \\ u_i(R - L + 1) \end{bmatrix} = Xf_i = \begin{bmatrix} u_i(1) & \cdots & x(L) \\ \vdots & \ddots & \vdots \\ x(R - L + 1) & \cdots & x(R) \end{bmatrix} \begin{bmatrix} f_i(1) \\ \cdots \\ f_i(L) \end{bmatrix} \quad (3)$$

Following this, the CK for each mode can be delineated as such:

$$CK_Q(u_i) = \frac{u_i^Q W_Q u_i}{u_i^H u_i} \quad (4)$$

where the Hermitian transpose operation is represented by H, and the weighted correlation matrix's interim variable is denoted by W_Q, are delineated in Equation (5):

$$W_Q = \begin{bmatrix} \left(\prod_{q=0}^{Q} u_i[1 - qT_S]\right)^2 & 0 & \cdots & 0 \\ 0 & \left(\prod_{q=0}^{Q} u_i[2 - qT_S]\right)^2 & \cdots & 0 \\ \vdots & \vdots & \ddots & \vdots \\ 0 & 0 & \cdots & \left(\prod_{q=0}^{Q} u_i[R - L + 1 - qT_S]\right)^2 \end{bmatrix} = \frac{1}{\sum_{r=1}^{R-L+1} u_i[r]^{Q-1}} \quad (5)$$

Combining Equations (3) and (4), we obtain the final expression of the objective function:

$$CK_Q(u_i) = \frac{f_i^H X^H W_Q X f_i}{f_i^H X^H X f} = \frac{f_i^H P_{XWX} f_i}{f_i^H P_{XX} f_i} \quad (6)$$

The matrixes P_{XWX} and P_{XX} signify weighted correlation matrixes and correlation matrixes in their respective roles. So far, according to the solution of Equation (1), the revised method for the k th filter coefficient has been derived, and the single-component mode can be acquired through the utilization of the optimized FIR filter bank. However, since there may be multiple modulations of the signal, single-component modes extracted from the signal may contain the same fault characteristics, with some modes representing merely inconsequential noise components. To mitigate such redundancy and streamline computational processes, FMD employs an iterative procedure. During each iteration of the decomposition process, the two modes exhibiting the highest resemblance are initially identified, and the one with the lower associated kurtosis is removed.

When calculating the similarity of the two modes, a mode selection strategy that takes into account the multidomain mode similarity is proposed. Two modes $x_u(n)$ and $x_v(n)$ are assumed to be similar in the time domain, which is quantified by the temporal correlation coefficient (CC) as defined in the following equation:

$$CC_{uv} = \frac{\sum_{n=1}^{N} (x_u(n) - \bar{x}_u)(x_v(n) - \bar{x}_v)}{\sqrt{\sum_{n=1}^{N} (x_u(n) - \bar{x}_u)^2} \sqrt{\sum_{n=1}^{N} (x_v(n) - \bar{x}_v)^2}} \quad (7)$$

where the average value of the modes $x_u(n)$ and $x_v(n)$ are denoted by $\bar{x}_u$ and $\bar{x}_v$, respectively. Typically, CC values exceeding 0.7 generally indicate high similarity between the two compared modes, consistent with similarity metrics in other domains. After that, the reconstructed signal could be obtained by the decomposed signals.

Spectral subtraction method

In the signal processing process of mechanical equipment, the use of healthy signals is particularly important in order to effectively remove noise and highlight fault characteristics. A health signal is a signal acquired under normal operating conditions and can characterize the typical state characteristics of the device, so it can be used as a reference for noise reduction.[34] The spectral subtraction method removes noise components by comparing the spectral differences between the healthy and fault signals, resulting in a clearer fault signal. The schematic of the principle of spectral subtraction is displayed in Figure 1. The steps and corresponding formulas for spectral subtraction are outlined below:

(1) Calculate the spectrum. The fault signal x_F and the health signal x_H are processed with a fast Fourier transform to get their spectral results:

$$\begin{aligned} X_{F_0}(f) &= FFT(x_F) \\ X_{H_0}(f) &= FFT(x_H) \end{aligned} \quad (8)$$

where $X_{F_0}(f)$ and $X_{H_0}(f)$ represent the spectrum of fault signals and health signals, respectively.

(2) Spectrum normalization. The spectrum is normalized so that its amplitude is limited to the range of [0,1], which is convenient for comparison and less impact of numerical differences. Normalized computational research is expressed as follows:

$$X_{F_0}{}^{norm}(f) = \frac{X_{F_0}(f) - \min(X_{F_0}(f))}{\max(X_{F_0}(f)) - \min(X_{F_0}(f))} \quad (9)$$

$$X_{H_0}{}^{norm}(f) = \frac{X_{H_0}(f) - \min(X_{H_0}(f))}{\max(X_{H_0}(f)) - \min(X_{H_0}(f))} \quad (10)$$

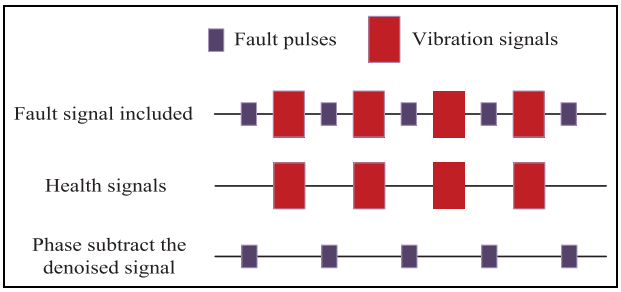

Figure 1. Schematic of spectral subtraction.

Here, $X_{F_0}{}^{norm}(f)$ and $X_{H_0}{}^{norm}(f)$ denote the normalized fault and health signal spectrum, respectively.

(3) Subtraction of spectrum. To obtain the desired result, the normalized spectrum $X_{F_0}{}^{norm}(f)$ of the healthy signal is deducted from the spectrum of the fault signal, ensuring that any resulting negative values are set to zero to avoid invalid outputs,

$$D(f) = \max(0, X_{F_0}{}^{norm}(f) - X_{H_0}{}^{norm}(f)) \quad (11)$$

The $D(f)$ obtained in this manner eliminates the healthy signal components in the differential spectrum and highlights the fault information.

(4) Inverse transformation back to the time domain. Finally, the inverse fast Fourier transform is performed on the difference spectrum $D(f)$, and the processed time-domain signal is as follows:

$$\hat{x}(t) = IFFT(D(f)) \quad (12)$$

This healthy signal-based spectral subtraction method significantly reduces the impact of noise and enhances fault features, making mechanical fault diagnosis in complex environments more reliable.

The proposed method

According to the theoretical basis of the previous "Feature mode decomposition" and "Spectral subtraction method,"Figure 2 provides a comprehensive illustration of the workflow for the introduced method. First, the Optimal Weight Sensing Index (OWSI) is used to evaluate the sensitivity of the modes to the fault, and the nonstationarity of the quantified signal of the impact feature is detected by the CK measurements, so as to preliminarily screen out the number of effective modes and obtain the parameters required for

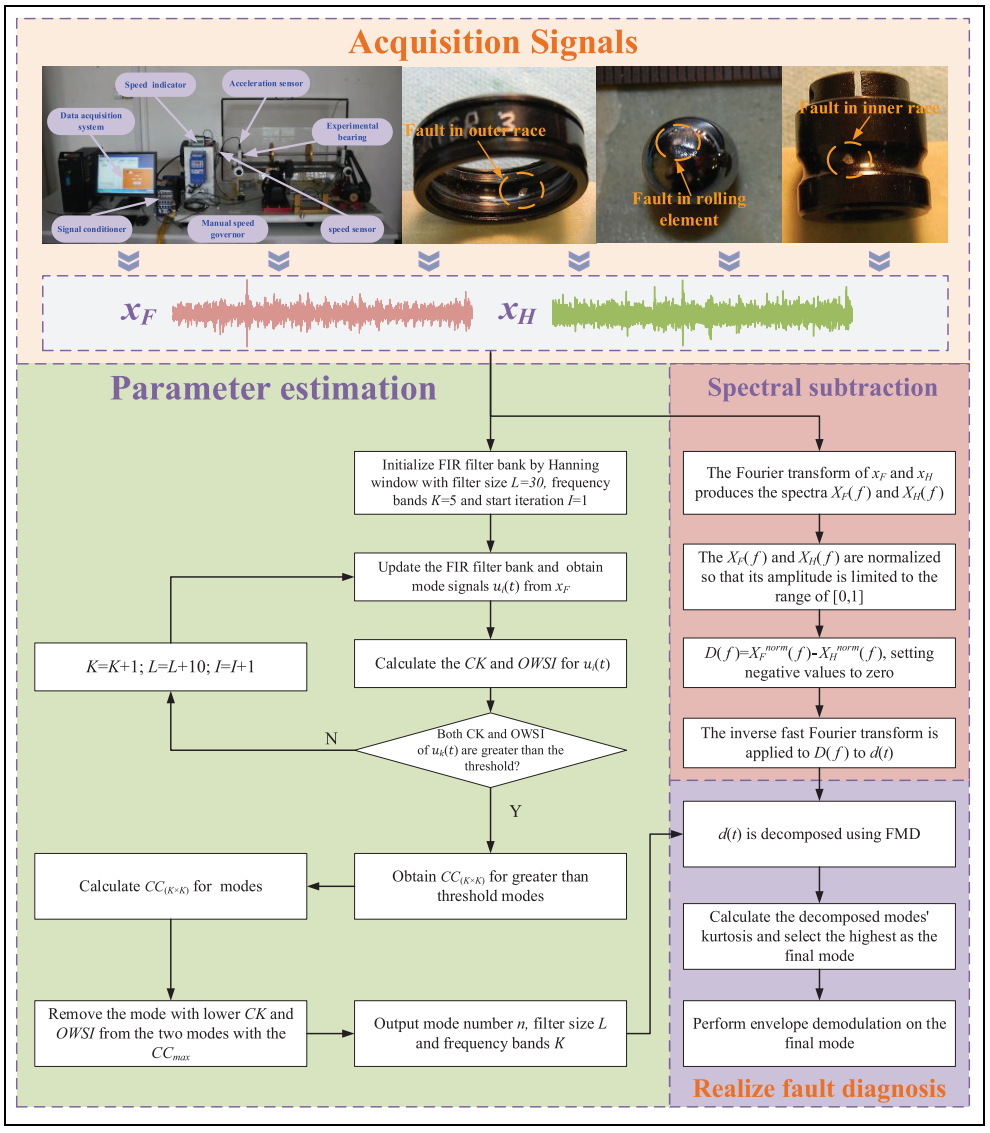

Figure 2. The proposed method flowchart.

the FMD accordingly. The FMD is then used to decompose the signal processed by spectral subtraction. Finally, the effective modes are selected according to the kurtosis index, and the envelope demodulation is carried out to complete the fault diagnosis. The detailed workflow of the proposed method is outlined below to illustrate its implementation:

Step 1: The fault signal x_F and health signal x_H are sampled from the test bench.
Step 2: Input the parameters, including the filter size $L = 30$ (According to reference Miao et al.,[23] the filter length L for FMD should ideally fall within the range of [30–100]. Hence, the initial filter length L in this study is chosen to be 30, frequency bands $K = 5$, and the maximum iteration number $I_{\max}$. Initialize the iteration process by setting $I = 1$).
Step 3: Initialize the FIR filter bank using the Hanning window, configured according to the provided input parameters.
Step 4: Filter the fault signal x_F through the FIR filter bank to obtain the decomposed modes $u_i(t)$, where $i = 1, 2, \ldots, i$.
Step 5: Calculate CK and $OWSI$ for the modes.

$$CK = \frac{\sum \left(\prod_{q=0}^{Q} x(r - qT) \right)^2}{\left(\sum x(r)^2 \right)^{Q+1}},$$

where Q represents the lag number, which is used to define the number of product terms; T is the period:

$$OWSI = \sum_j w_j \cdot |X_{F_0}(j) - X_{H_0}(j)|,$$

where w_j denotes the weight factor of the jth component, calculated from the difference between the normalized amplitude spectra of the x_F and x_H.

Step 6: Check CK and $OWSI$ thresholds. Judge whether the CK and $OWSI$ values are greater than thresholds (average value). If not, update the parameters $L = L + 10$; $K = K + 1$, set $I = I + 1$. If yes, proceed to step 7.
Step 7: Calculate $CC_{(K \times K)}$ matrix and remove redundant modes. Lock the two modes that demonstrate the highest CC values to preserve their significance. Then, the mode with the lesser of both CK and $OWSI$ is discarded from the two modes. Highly correlated modes are removed first to ensure the independence of the modes.
Step 8: Output the final results. Output the final decomposed modes n, the filter size L, and the frequency bands K.
Step 9: Decompose the signal $d(t)$ by FMD according to the parameters to get n modes. The x_F and x_H are processed by spectral subtraction to obtain $d(t)$.
Step 10: Determine the final mode. Calculate n modes' kurtosis and select the highest as the final mode.
Step 11: The final obtained mode components are demodulated by envelope to extract fault features and realize fault diagnosis.

Simulation analysis

To validate the effectiveness of the proposed method, simulated signals are constructed. These signals comprise three key components: the bearing fault impulse signal $s(t)$, the rotational frequency signal $c(t)$, and the white noise $n(t)$. The overall signal can be represented in the following form:

$$x(t) = s(t + \Phi) + c(t) + n(t) \tag{13}$$

where $\Phi = 0.01$ s indicates the repetition interval of the fault impacts, $s(t)$ is modeled as a damped cosine function with an exponential decay factor and frequency component. The expression for $s(t)$ is

$$s(t) = e^{-2\pi f_n \tau t} \cdot \cos(2\pi f_n t) \tag{14}$$

In this expression, $f_n = 5000$ Hz, $\tau = 0.02368$, rotational frequency signal $c(t)$, representing normal operating conditions, is constructed from the fundamental frequency and multiple harmonics, as follows:

$$c(t) = 0.3 \sin(4\pi f_r t) + 0.15 \sin(6\pi f_r t) + 1.5 \sin(2\pi f_r t) \tag{15}$$

Here, $f_r = 30$ Hz is the fundamental frequency, and the higher-order harmonics (second and third harmonics) represent the rotational frequency and its associated mechanical vibrations. Additionally, Gaussian white noise $n(t)$ is incorporated into the simulated signal, resulting in an signal-to-noise ratio at -17.4096 dB. Based on this structure, two types of signals are defined:

Fault Signal $x_F(t)$: This signal includes the fault impulse, rotational frequency, and noise, defined as follows:

$$x_F(t) = s(t + \Phi) + c(t) + n(t) \tag{16}$$

Healthy Signal $x_H(t)$: This signal consists only of the rotational frequency and noise, defined as follows:

$$x_H(t) = c(t) + n(t) \tag{17}$$

This study adopts a sampling frequency of 25.6 kHz, and the simulated signal is displayed in Figure 3(a) for demonstration. Fourier transform and Hilbert envelope spectrum analysis are widely applied for fault feature extraction. When no prior information is available, envelope demodulation is usually performed over the entire frequency range. In such cases, the spectral lines of interest are often masked by noise spectral lines, as shown in Figure 3(b). The proposed method fully decomposes the raw signal, highlighting fault related information. Figure 4 displays the fault components extracted by the proposed method, along with the fault characteristic frequencies (FCFs) of 100 Hz and their harmonic frequencies (200 Hz,

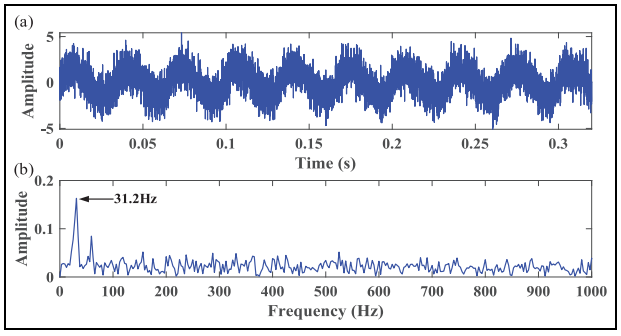

Figure 3. Simulation signal: (a) Raw signal and (b) Envelope spectrum.

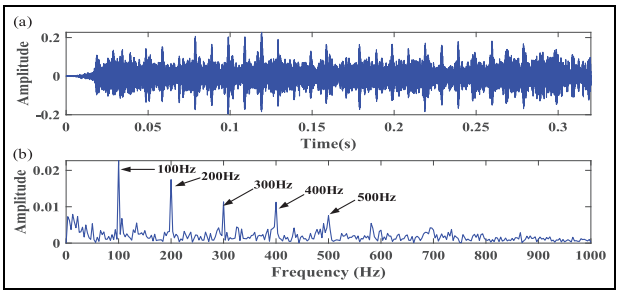

Figure 4. Processing the simulated signal by the proposed method: (a) Decomposed signal and (b) Envelope spectrum.

300 Hz, 400 Hz, etc.), which are distinctly visible in Figure 4(b).

To verify the effectiveness of the proposed method, a comparison is carried out with five alternative methods, as described below:

(1) *FMD Method:* The FMD method decomposes the fault signal into multiple components, corresponding to the number of modes specified in the FMD. The parameter n in FMD is directly linked to the determination of fault information extraction. To ensure effective signal decomposition,[23] the parameter n is set to 3 in this comparison experiment.

(2) Sparse Random Mode Decomposition (SRMD) Method: The latest SRMD is mainly used to decompose signals through sparse representation and random feature generation.[33] SRMD can extract effective features in noisy environments while ignoring irrelevant modes, thus realizing efficient fault diagnosis of signals. Therefore, it is one of the comparison methods in this article.

(3) *SGMD Method:* The signal can be decomposed into multiple components using SGMD. The kurtosis values of all components are computed, and the component with the highest kurtosis is identified and chosen as the fault component for subsequent analysis.

(4) *VMD Method:* A fault signal is divided into several components through VMD, with the early components generally containing the relevant fault information. Due to space constraints, only the initial three components are analyzed in this study.

(5) *EMD Method:* The fault signal is decomposed using EMD to obtain multiple components. Similar to VMD, only the initial three components are analyzed in this study.

The FMD analysis results are shown in Figure 5. The FMD decomposes a signal through frequency band segmentation and iterative adaptive adjustment. As the decomposition progresses, high-frequency oscillations are gradually suppressed, leaving primarily low-frequency, slowly varying components in the residual signal. This process results in a progressively smoother signal in the decomposition output. It is worth mentioning that FCF is observed only in mode #1 within the envelope spectra of these three components, and its intensity is barely noticeable.

The decomposition results of the SRMD for the simulated signal are shown in Figure 6(a). Through sparse representation and mode dictionary construction, critical frequency features are effectively extracted from the signal, and FCFs are precisely detected. The fault component signal in the time domain is presented, with sparse features extracted by SRMD. The envelope spectrum corresponding to Figure 6(a) in the frequency

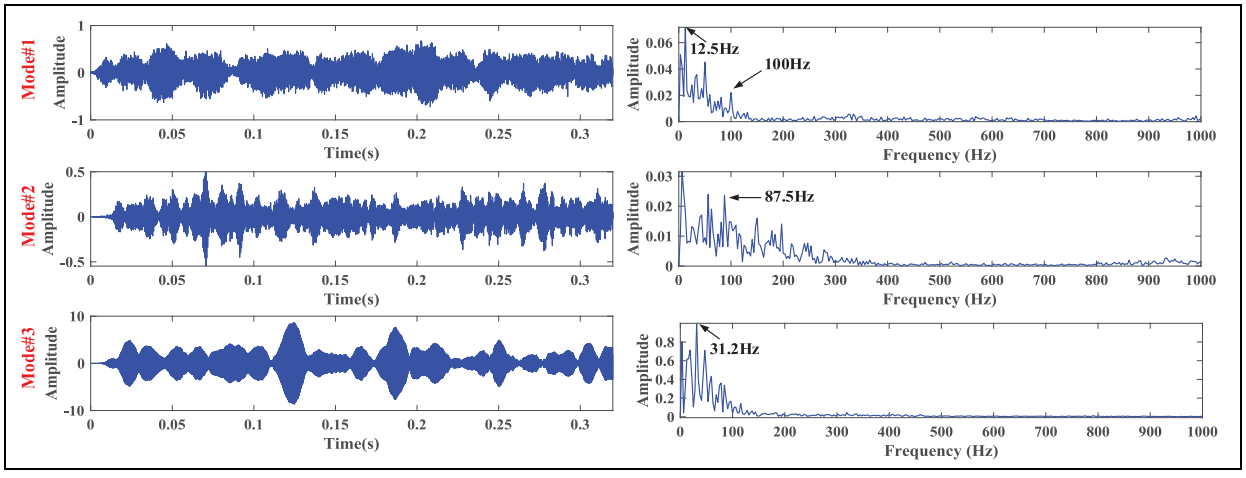

Figure 5. FMD decomposition result with n = 3 for the simulated signal.
FMD: Feature mode decomposition.

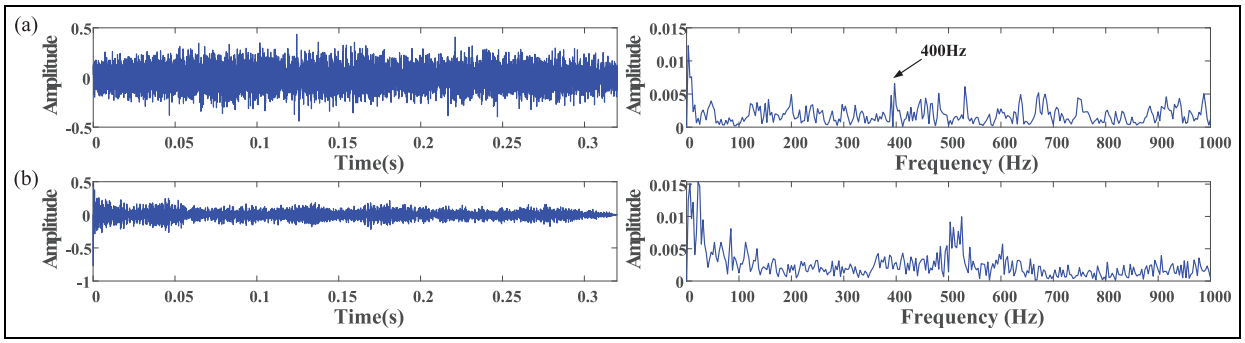

Figure 6. SRMD and SGMD deal with simulation signal: (a) SRMD and (b) SGMD.
SGMD: Symplectic geometric mode decomposition; SRMD: Sparse random mode decomposition.

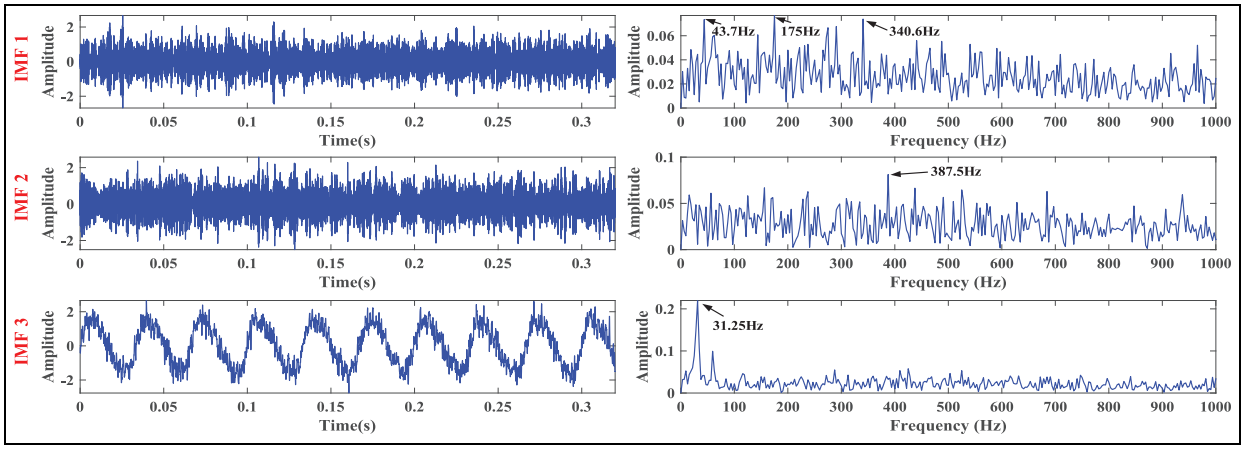

Figure 7. The initial three components from the VMD analysis of the simulation signal.
VMD: Variational mode decomposition.

domain is displayed, where a prominent peak at 400 Hz is observed, though it is nearly obscured by noise.

SGMD can decompose a simulated signal into multiple components. Due to the impact of space, this article selects the effective components according to the principle of peak maximum. In general, the larger the peak of the component, the richer the fault information. The simulated signal's analysis results obtained through SGMD are presented in Figure 6(b). The fault components are extracted in Figure 6(b), which maintain the geometry and dynamics of the signal, exhibiting sparse fluctuations. Figure 6(b) shows the corresponding envelope spectrum, which is not effectively extracted so that the fault frequency is multiple. Figure 7 presents the results derived from VMD based on kurtosis analysis. The FCF is entirely absent in the envelope spectrum. Because relevant parameters need to be set in VMD, performance will deteriorate if parameters are not chosen appropriately.

The results of EMD are the same as those of VMD. The fault signal is decomposed into nine components by EMD, with the initial three are displayed in Figure 8. The components are organized in order of decreasing frequency and represent the original fault signal processed through various bandpass filters. Envelope demodulation is applied to isolate specific FCFs. As shown in Figure 8, the FCF at 100 Hz, along with its harmonics at 300 Hz and 500 Hz (marked with red circles), is detected exclusively in the envelope spectrum of the third component, where significant noise interference is also evident.

From the simulated signal analysis above, the following conclusions can be drawn: (1) Fault features are extractable by the proposed method, even under certain levels of noise interference; (2) Insufficient decomposition is achieved by techniques like SRMD and SGMD, making them incapable of extracting fault features when noise interference is present; (3) The decomposition effects of FMD, VMD, and EMD are highly dependent on parameters, making them susceptible to noise interference, which affects their stability and reliability in practical applications; (4) Fault information is

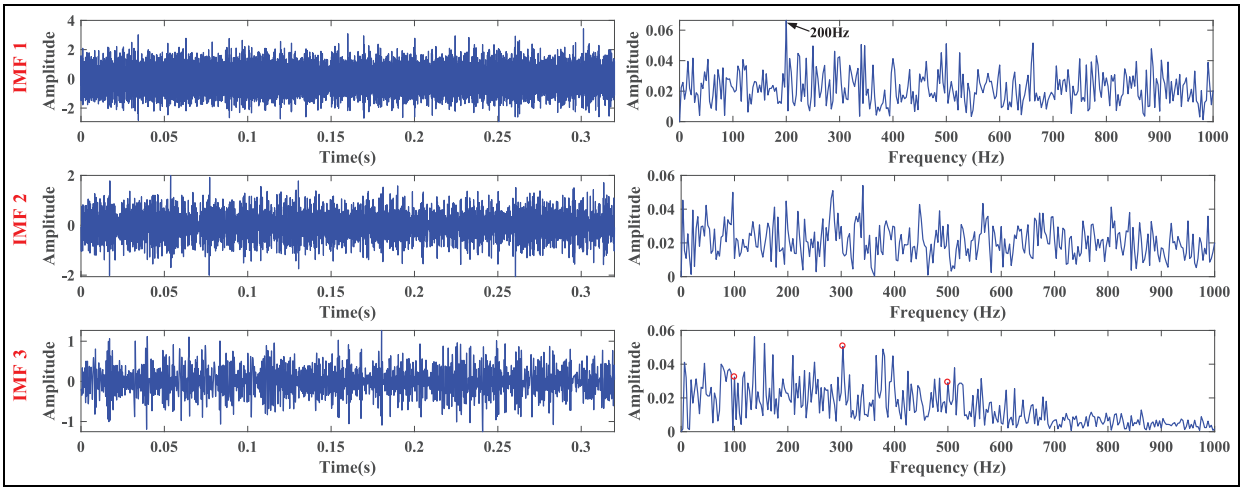

Figure 8. The initial three components from the EMD analysis of the simulation signal.
EMD: Empirical mode decomposition.

emphasized, and noise influence minimized by using the decomposition strategy based on spectral subtraction.

Experimental case study

This section presents an evaluation performance of the proposed method on experimental signals. For this purpose, the method is applied to three type datasets: experimentally collected bearing fault data, engineering bearing fault data, and publicly·bearing fault data. By analyzing these three datasets, the effectiveness and applicability of the method is thoroughly assessed.

Self-built experimental dataset

(1) ***Experimental Equipment***: The setup of the bearing fault test bench is depicted in Figure 9, with further details provided in Liu and Xiang[40] and Meng et al.[41]. Figure 10 illustrates the positions of bearing faults, which include the inner race, outer race, and rolling elements. Key bearing parameters are listed in Table 1. Vibration signals are recorded during the experiment using an acceleration sensor. The recorded signal contains 8192 data points, with the sampling frequency set to $f_s = 25.6$ kHz. BPFI presents the ball pass frequency on inner race, and BSF presents the ball spin frequency, f_{shaft} notes the shaft speed. Furthermore, the theoretical FCF is determined using the equation outlined in Table 2.

(2) ***Inner Race Fault Analysis***: The inner race signal of the bearing collected during the experiment is displayed in Figure 11. The rotational frequency for this experiment is 39.84 Hz. Based on the values in Table 2, the FCF of the inner race is calculated to be 196.8 Hz. However, analysis of the signal's envelope spectrum reveals only the rotational frequency, making it difficult to confirm the fault exists.

To diagnose potential faults, the proposed approach is employed to examine the collected signals, following a similar process as previously described. In the bearing fault experiment, both faulty and healthy signals are acquired and processed with proposed method. The decomposed signal derived and the final analysis results are presented in Figure 12. The proposed method accurately extracts the FCF of the bearing's inner race at 196 Hz, along with its harmonics at 393.8 Hz, 590.6 Hz, and 784.4 Hz. While the FCF value shows a slight deviation from the theoretical value, it remains within an acceptable range of error.

A comparative analysis using FMD, SRMD, SGMD, VMD, and EMD is performed to highlight the advantages of the proposed method. The results from five methods are shown in Figures 13–16. For FMD, multiple peaks are observed, suggesting potential mode aliasing during decomposition, as well as possible modulation effects and noise interference in the analysis of bearing faults. The SRMD decomposition results are consistent with the findings from the previous section, showing limited capability in extracting fault feature components. While the FCF is extracted by the SGMD algorithm, it is significantly affected by noise interference. The Intrinsic Mode Functions 2 (IMF2) envelope spectrum from VMD only captures the rotational frequency, failing to extract the FCF. Similarly, the EMD decomposition results in gradual signal smoothing and can only capture the rotational frequency across multiple components.

Table 1. Mechanical properties of the bearing.

Parameter	Value	Parameter	Value
Bearing mean diameter (D)	33.47 mm	Number of balls (n)	8
Ball diameter (d)	7.93 mm	Contact angle (α)	0°

Table 2. Formulas for calculation.

Frequency	BPFI	BPFO	BSF
Value	$4.94 \times f_{shaft}$	$3.05 \times f_{shaft}$	$1.99 \times f_{shaft}$

BPFI: ball pass frequency on inner race; BPFO: ball pass frequency on outer race; BSF: ball spin frequency.

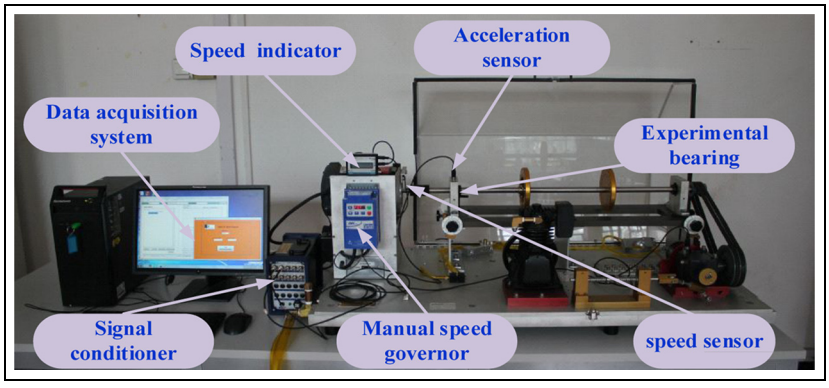

Figure 9. Test bench.

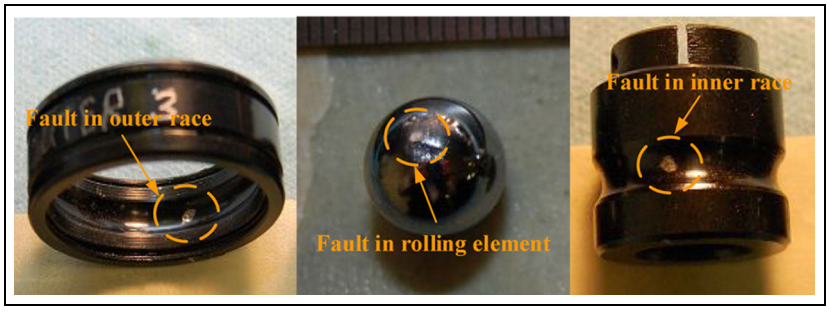

Figure 10. Fault in bearing.

Evidently, complete signal decomposition is not achieved by the comparison methods, leaving the decomposed components with substantial noise interference. In contrast, spectral subtraction is employed in the decomposition strategy of the proposed method to enhance fault information, providing continuous guidance for signal decomposition. Ultimately, the fault is successfully diagnosed only by the proposed method.

(2) ***Compound Fault Analysis***: In this section, the compound fault signal analyzed is collected at a rotational frequency of 49.80 Hz. This compound fault primarily includes both outer race and inner race faults. The corresponding FCF for both can be calculated using the values provided in Table 2, which are 151.9 Hz and 99.1 Hz, respectively. The results of the Hilbert envelope spectrum analysis directly on compound fault are

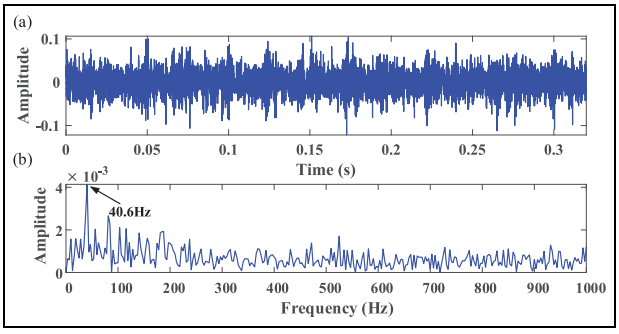

Figure 11. Inner race fault signal: (a) Raw signal and (b) Envelope spectrum.

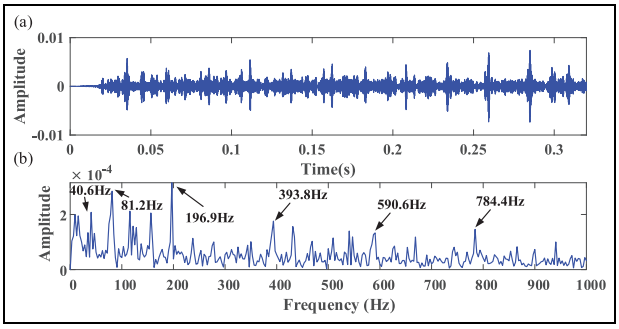

Figure 12. Processing the inner race fault signal by the proposed method.: (a) Decomposed signal and (b) Envelope spectrum.

shown in Figure 17(b). It can be observed that 100 Hz and 200 Hz are the FCFs of the rolling elements, and the FCFs of the outer ring faults are not identified; therefore, further analysis and processing of the signal is required.

The compound fault signal is processed by the proposed method. The decomposed signal derived and the final analysis results are presented in Figure 18. This method is used to effectively determine the FCF of all fault types. In Figure 18(b), the FCFs of the rolling elements at 100 Hz and its harmonic at 200 Hz, as well as the FCF of the outer race at 150 Hz and its harmonic at 300 Hz, are displayed, all corresponding to a rotational frequency of 50 Hz. As a result, the presence of a compound fault within the bearing can be confirmed.

To evaluate the advantages of the proposed method in diagnosing compound fault, a performance comparison is conducted using FMD, SRMD, SGMD, VMD, and EMD. The results from five procedures are displayed in Figures 19–22. When the signal is decomposed using FMD, three mode components are obtained, similar to the previous case, and fault features cannot be extracted effectively. In the envelope spectrum obtained after SRMD decomposition of the signal, some peaks are observed, but none correspond to the FCFs. The SGMD component that is most likely to contain fault information is selected according to the kurtosis principle, and the resulting plot corresponding to the fault component in Figure 20(b) only finds a peak value of 100 Hz, so it is possible to detect the FCF of the rolling element.

When using VMD to decompose signals, the initial three components are used. In IMF1, 50 Hz and 100 Hz can be observed, which indicates that the rotational frequency and its harmonics are extracted, and of course, the FCF of the rolling element may also be extracted. However, in IMF2, only a rotation frequency of 50 Hz can be observed. In the results corresponding to the IMF3 component, the rotational frequency and rolling body FCF can be clearly seen, but the outer race fault is only visible at 150 Hz, with no FCF observed at 300 Hz. Thus, the IMF3 component is more likely to indicate that only the rotational frequency, rolling element FCF, and its harmonics are extracted. When using EMD to decompose the signal, a certain FCF can be extracted in all three components. Although the rolling body FCF and outer race FCF can be extracted in IMF3, the corresponding harmonics cannot be extracted. Additionally, the signal gradually tends to be smoothed, making this method relatively ineffective compared to the proposed method.

This section describes the diagnostic results of two single fault signals (outer race fault and rolling element fault) with a rotation frequency of 39.84 Hz in the self-built dataset. From the formula in Table 2, the FCFs are calculated as 121.5 Hz for the bearing's outer race and 79.3 Hz for the rolling elements. Due to the limitation of space in this article, only the results of the proposed method are given here, as shown in Figure 23. It mainly includes the original signals of the two fault signals, the decomposition signal processed by the proposed method, and the final result graph. In the results of the outer race signal in Figure 23(c), the FCF of 118.8 Hz and its double frequency of 237.5 Hz of the outer race can be identified, confirming the existence of an outer ring fault in the bearing. Similarly, its FCF of 81.2 Hz and doubling of 161.3 Hz can be found in the rolling element diagnostic results in Figure 23(c). It has been observed that the FCF values slightly deviate from the theoretical values, but they are within the error margin considered acceptable.

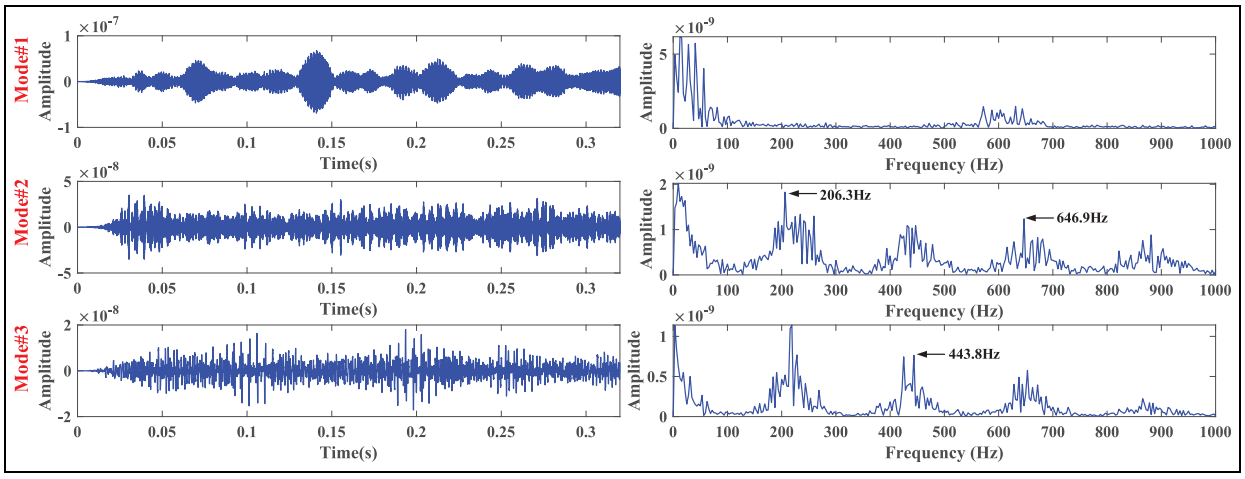

Figure 13. FMD decomposition result with $n = 3$ for the inner race fault signal.
FMD: Feature mode decomposition.

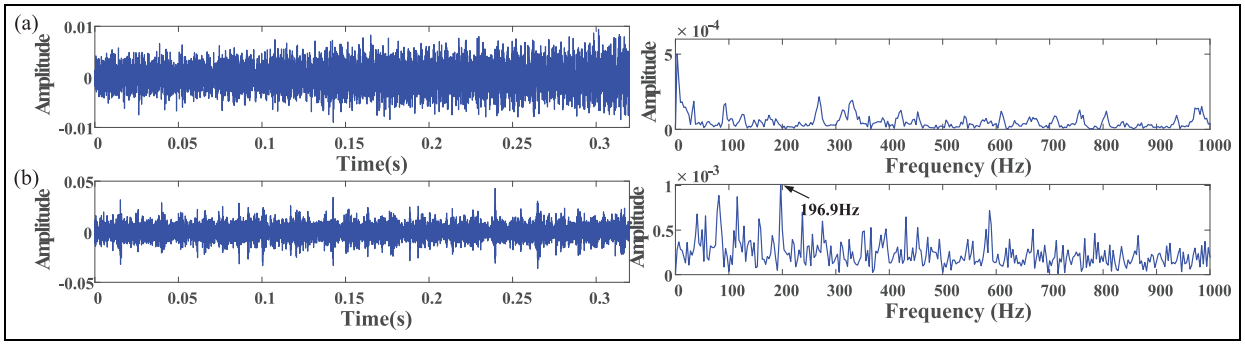

Figure 14. SRMD and SGMD deal with the inner race fault signal: (a) SRMD and (b) SGMD.
SGMD: Symplectic geometric mode decomposition; SRMD: Sparse random mode decomposition.

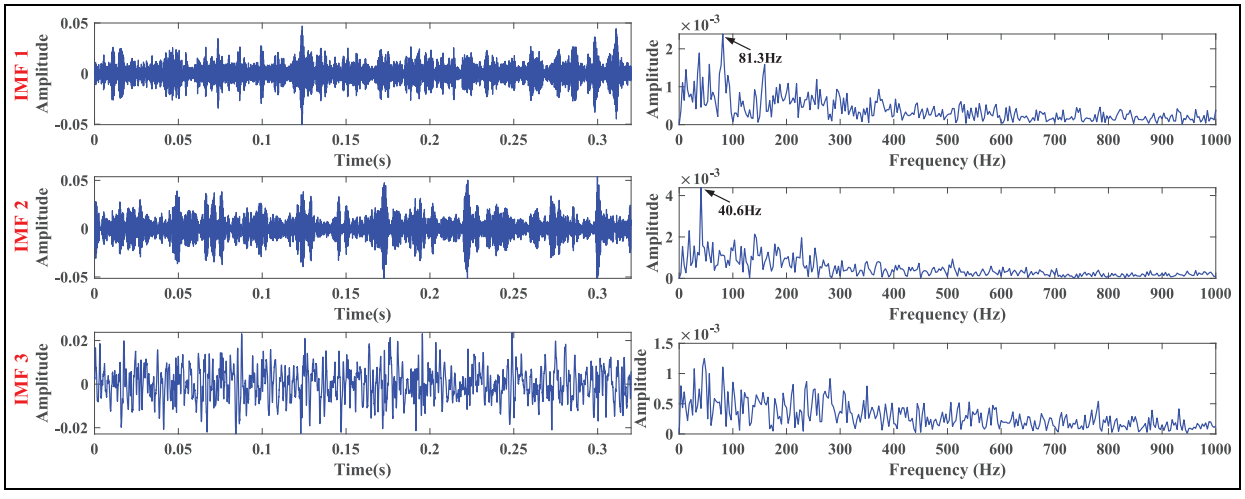

Figure 15. The initial three components from the VMD analysis of the inner race fault signal.
VMD: Variational mode decomposition.

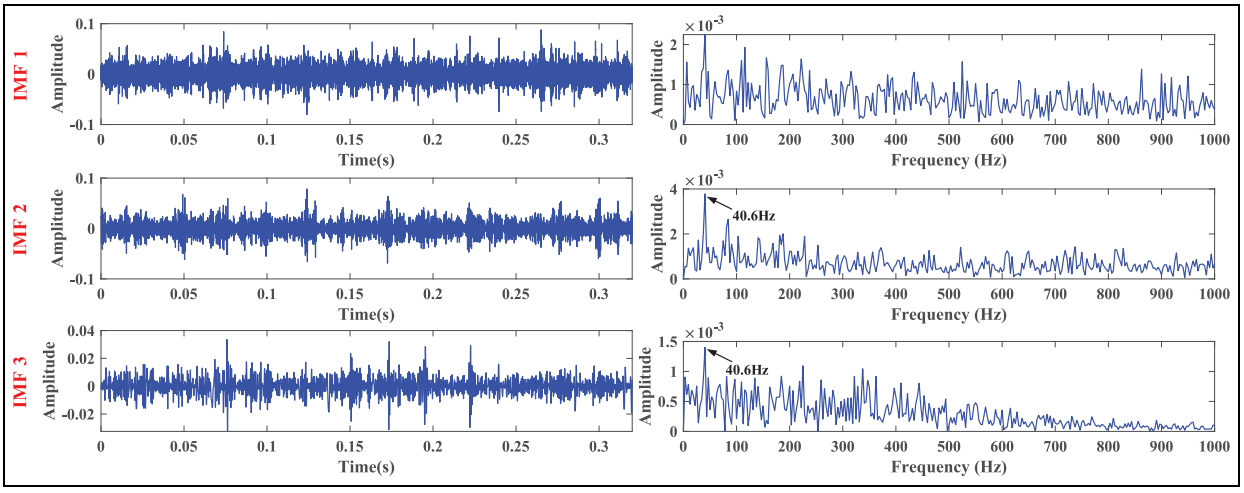

Figure 16. The initial three components from the EMD analysis of the inner race fault signal.
EMD: Empirical mode decomposition.

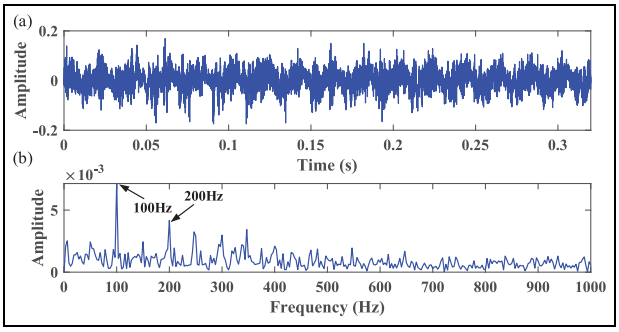

Figure 17. Compound fault signal: (a) Raw signal and (b) Envelope spectrum.

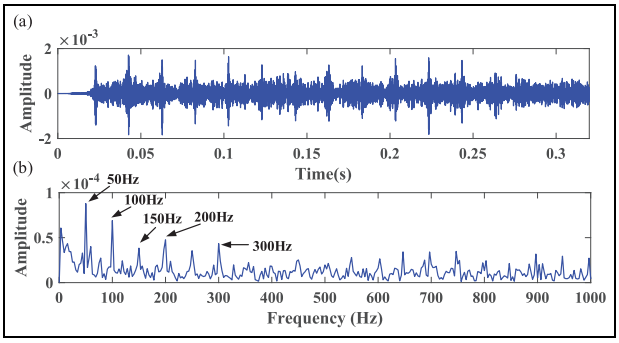

Figure 18. Processing the compound fault signal by the proposed method: (a) Decomposed signal and (b) Envelope spectrum.

Engineering data

To correspond with practical application contexts, this part will focus on analyzing the operational monitoring data of a company's water pump. As a key experimental subject, this water pump mainly serves to deliver the stable water flow needed by the system, thus guaranteeing the normal operation of various associated devices. In industrial production and water treatment systems, water pumps powered by motors transport water from regions with lower pressure to those with higher pressure. For this reason, the normal operation of the pump is vital to maintaining the overall efficiency and stability of the entire system. In the experiment, the monitoring data gathered from the motor's drive end will be utilized to conduct a thorough analysis of the pump's operating status. It should be noted that due to confidentiality regulations, a detailed account of the experimental equipment cannot be provided here. Figure 24 illustrates the real time operational status during data collection, highlighting the primary components, which include the motor and pump. The experimental setup for inducing an outer race fault in the SKF 6317/C3 rolling bearing is provided in Figure 25.

For this experimental data acquisition, sampling is conducted at a frequency of 51.2 kHz, yielding a total of 16384 data points. The bearing's rotational frequency is recorded at 46.8 Hz. The bearing's specifications and details are included in Table 3. By employing the mechanical parameters provided in Table 3, the fault frequency corresponding to the bearing's outer race can be determined. The computed FCFs are detailed in Table 4. BPFO presents the ball pass frequency on outer race. This analysis, based on real-world operational data, underscores the practical relevance and application of the theoretical framework discussed.

The raw signal of the engineering data along with its corresponding envelope spectrum are illustrated in Figure 26. No meaningful information can be

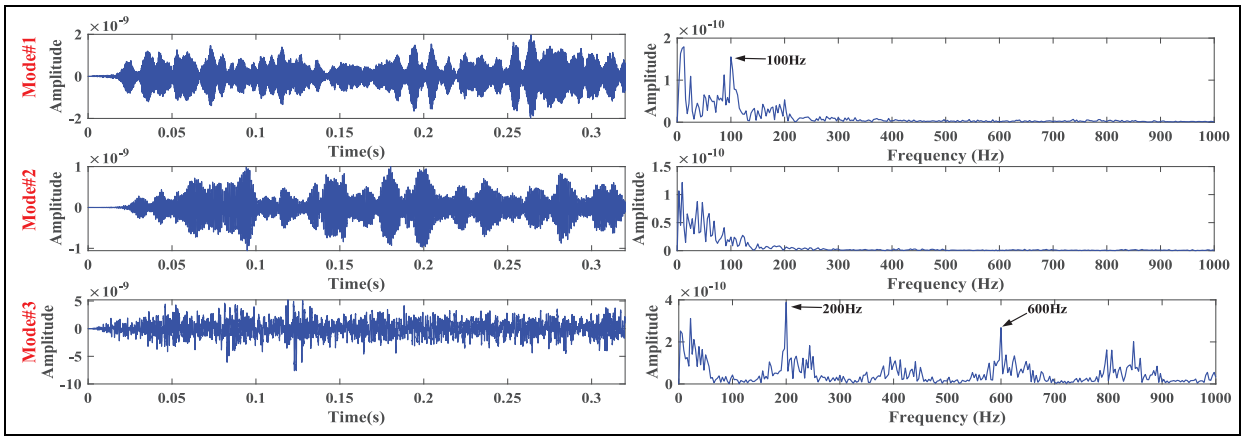

Figure 19. FMD decomposition result with $n = 3$ for the compound fault.
FMD: Feature mode decomposition.

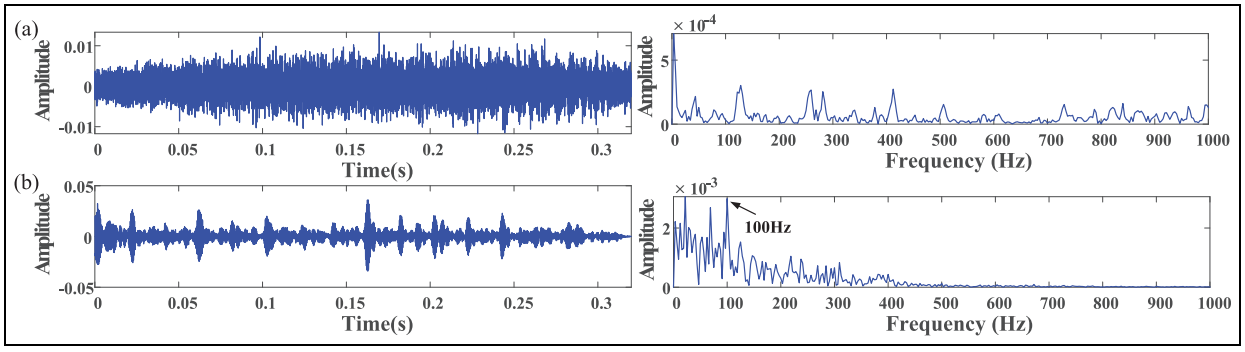

Figure 20. SRMD and SGMD deal with compound fault: (a) SRMD and (b) SGMD.
SGMD: Symplectic geometric mode decomposition; SRMD: Sparse random mode decomposition.

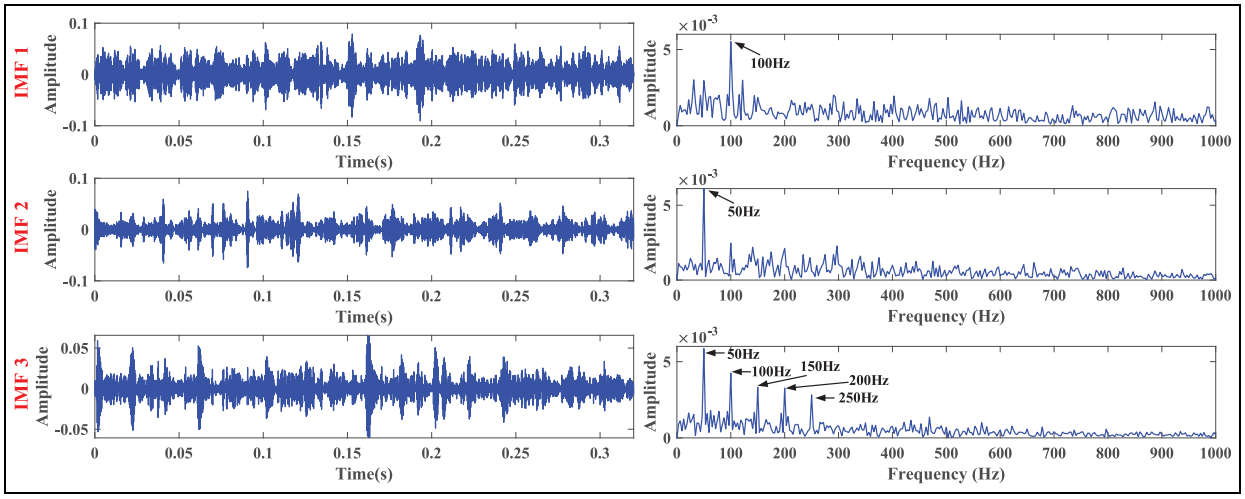

Figure 21. The initial three components from the VMD analysis of the compound fault signal.
VMD: Variational mode decomposition.

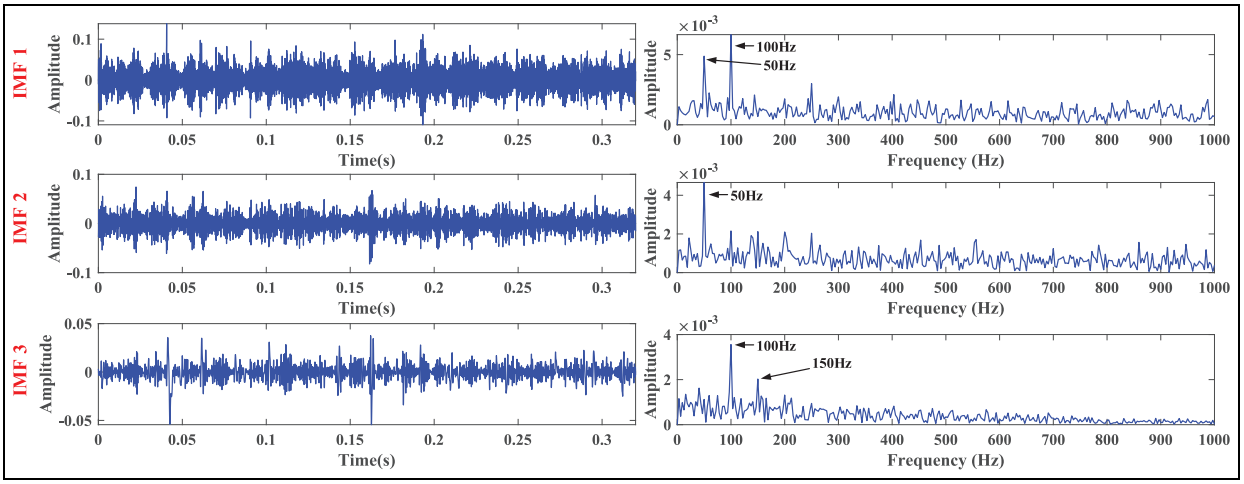

Figure 22. The initial three components from the EMD analysis of the compound fault signal.
EMD: Empirical mode decomposition.

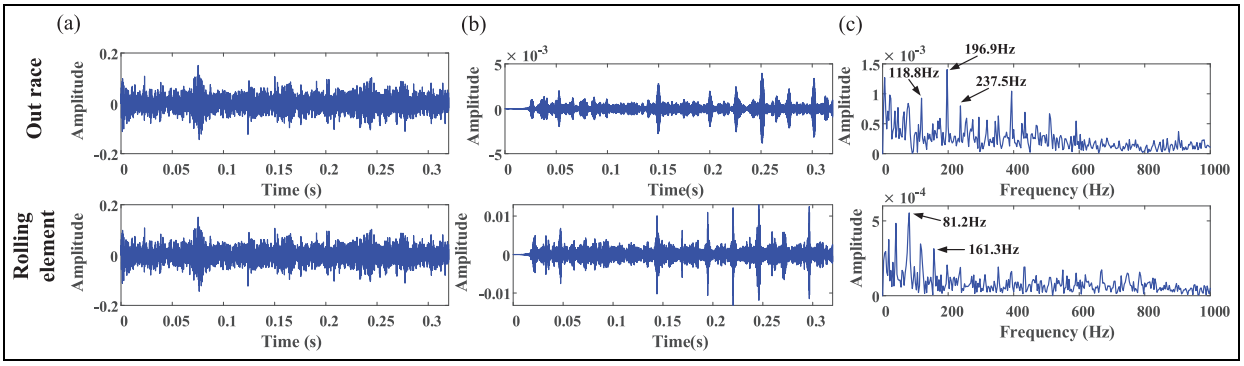

Figure 23. The proposed method deals with outer race signal and rolling elements signal: (a) Raw signal and (b) Decomposed signal and (c) Envelope spectrum.

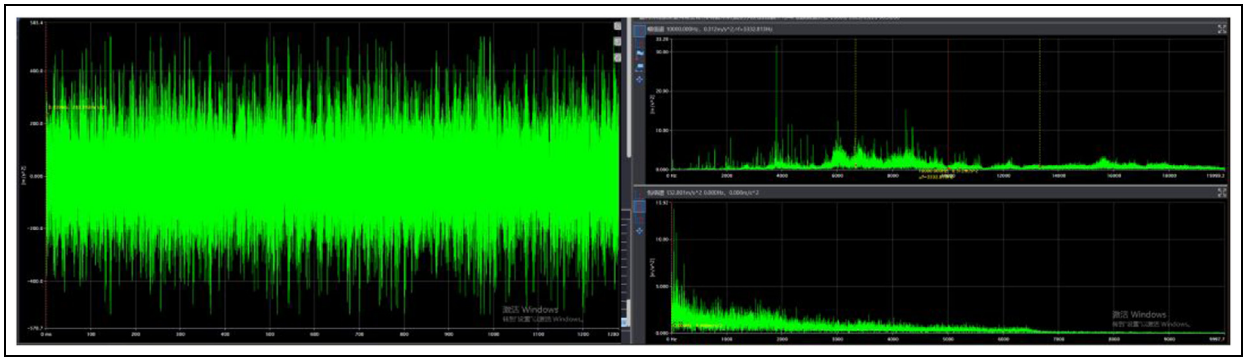

Figure 24. Signal acquisition system page.

extracted, as seen in Figure 26(b). It's challenge to expose the fault information in spectrum with prior signal processing techniques.

The proposed method is utilized for fault diagnosis of engineering data, and as shown in Figure 27(b), the FCF of 146.9 Hz and its harmonics (295.3 Hz,

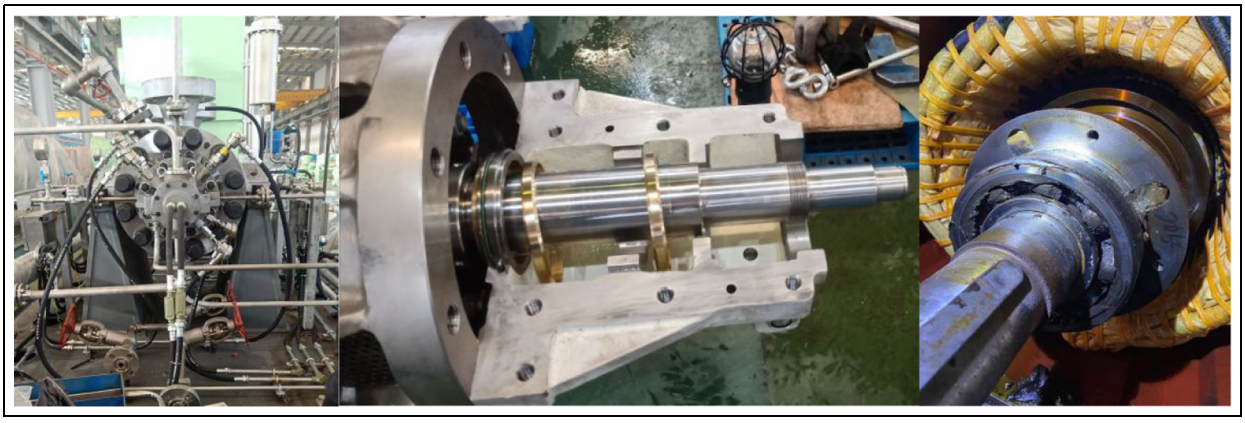

Figure 25. Related experimental setup.

Table 3. Mechanical properties of the bearing.

Parameter	Value	Parameter	Value
Bearing mean diameter (D)	132.5 mm	Number of balls (n)	8
Ball diameter (d)	30.16 mm	Contact angle (α)	0°

Table 4. The outer race fault frequency as well as its harmonics.

Frequency	BPFO	BPFO × 2	BPFO × 3
Value	144.8 Hz	289.6 Hz	434.4 Hz

BPFO: ball pass frequency on outer race.

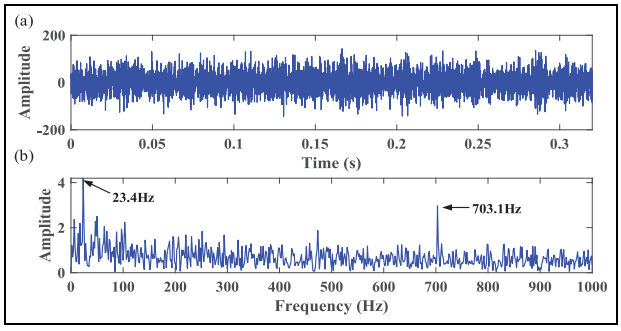

Figure 26. The engineering data signal: (a) Raw signal and (b) Envelope spectrum.

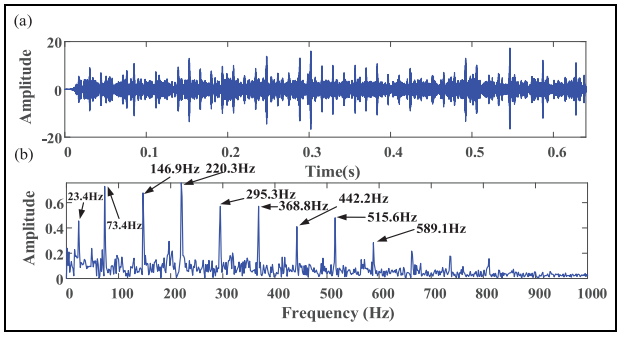

Figure 27. Processing the engineering data by the proposed method: (a) Decomposed signal and (b) Envelope spectrum.

442.2 Hz, 589.1 Hz) can be clearly observed. Furthermore, it is worth noting that a relatively high peak is observed around 146.9 Hz, and the corresponding frequency difference is exactly equal to 3/2 times the rotational frequency. This phenomenon indicates that during the operation of the bearing, when the fault

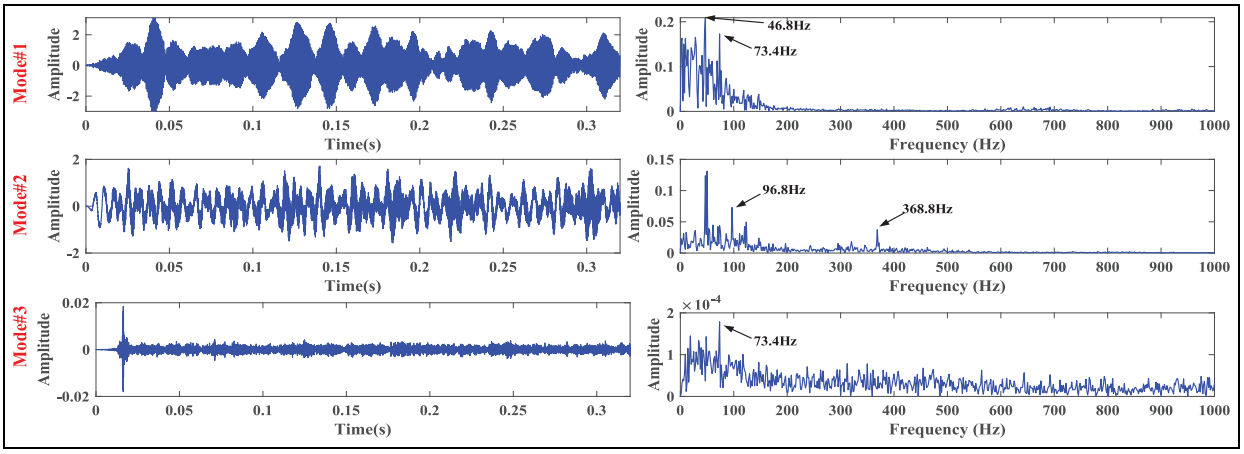

Figure 28. FMD decomposition result with $n = 3$ for the engineering data.
FMD: Feature mode decomposition.

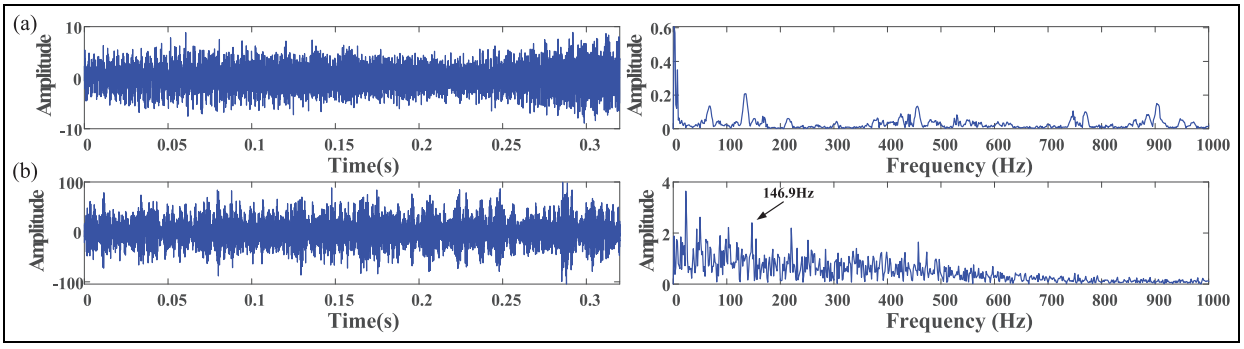

Figure 29. SRMD and SGMD deal with the engineering data: (a) SRMD and (b) SGMD.
SGMD: Symplectic geometric mode decomposition; SRMD: Sparse random mode decomposition.

interacts with the rotational frequency of the rotating components, sidebands centered at the FCF and spaced at intervals of $3/2\ f_r$ will be generated. Although the FCF values deviate slightly from the theoretical values, they remain within the acceptable error range.

The engineering bearing data are processed using five methods, following the same simulation analysis and experimental data analysis approaches as before. The processing results are shown in Figures 28–31. As illustrated in Figure 28, although each component shows a high amplitude, effective fault components are not successfully extracted.

Due to the inherent characteristics of SRMD, it is likely unsuitable for processing engineering data, as almost no useful information is visible. In Figure 29(b), the envelope spectrum indicates significant noise interference, and the fault frequency amplitude is not clearly observable. Compared to the proposed method, the performance is relatively poor. In VMD, only IMF2 extracts the FCF of 146.9 Hz, but its harmonics are severely affected by noise. Additionally, in the initial three components extracted using EMD, almost no useful fault information is observed, making fault diagnosis unachievable.

Overall, the proposed method demonstrates significantly better application performance in engineering practice than the other five methods. The method exhibits exceptional adaptability, capable of handling complex and variable real-world engineering scenarios, whereas other methods often show insufficient adaptability under similar conditions.

Publicly dataset

The public dataset used for bearing fault analysis in this section is the XJTU-SY dataset.[4] Detailed information regarding the test bench setup can be found in Chen and Feng.[41] In this study, the bearing outer race fault signal (file 125 of "Bearing1-2") and the healthy bearing signal (file 1 of "Bearing1-2") are utilized, with

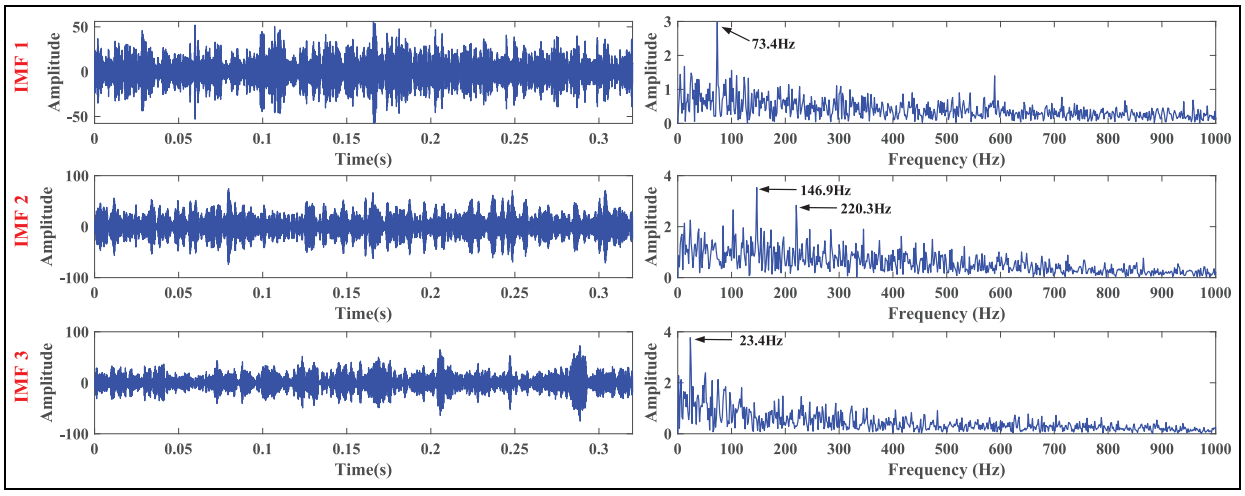

Figure 30. The initial three components from the VMD analysis of the engineering data.
VMD: Variational mode decomposition.

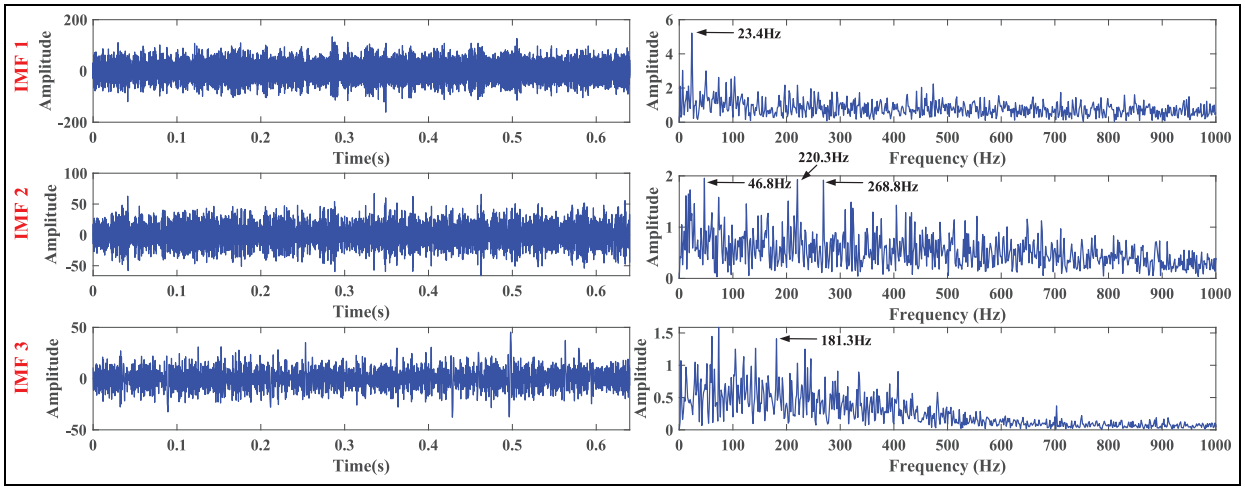

Figure 31. The initial three components from the EMD analysis of the engineering data.
EMD: Empirical mode decomposition.

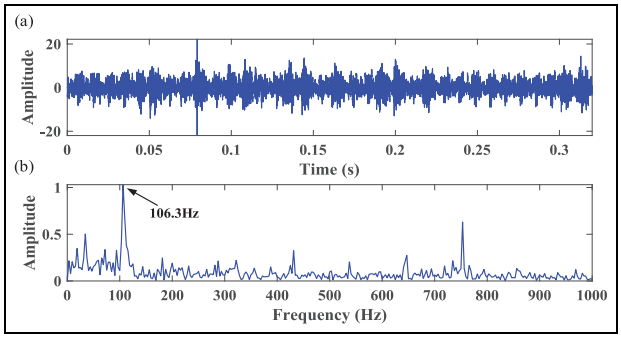

Figure 32. Signal and the corresponding envelop spectrum for the bearing with an outer race fault: (a) Raw signal and (b) Envelope spectrum.

the rotational frequency set to 35 Hz and the FCF to 107.9 Hz.

The collected bearing outer race fault signal is presented in Figure 32(a). In the envelope spectrum of this signal, only the first-order fault frequency is visible, while higher harmonics are masked by other components. To diagnose the outer race fault, the proposed method is applied to analyze the signal. The fault component is extracted and its corresponding envelope spectrum is shown in Figure 33. The first-order to seventh-order FCFs is successfully extracted by the proposed method, with minimal interference from noise spectral lines. Comparative analysis is performed using FMD, SRMD, SGMD, VMD, and EMD. The

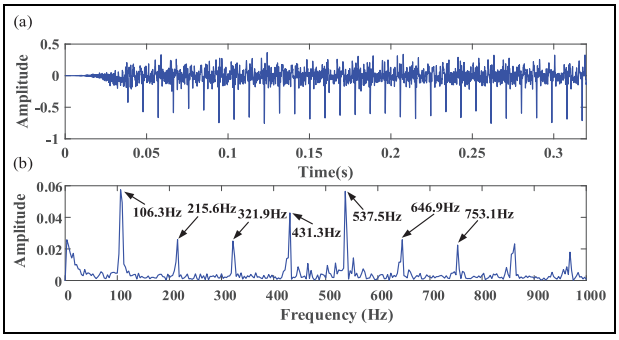

Figure 33. Analysis results of the proposed method for the bearing signal with an outer race fault: (a) Fault component and (b) Envelope spectrum.

results of these five methods are shown in Figures 34–37.

The third mode component of FMD extracts the FCF of the outer race of the bearing, but the amplitude is small and the multiplication of the rotational frequency is more prominent. The FCF of the outer ring is not extracted by SRMD, and the noise effect is larger. Three components are presented in the decomposition result of SGMD, none of which can be extracted from its envelope spectrum, so the fault component is selected according to the kurtosis principle. There is signal (red ellipse marked) distortion near the IMF1 and IMF3 FCFs of the VMD, and the FCF is only extracted in IMF2. In signal processing using EMD, the first-order FCF can be obviously extracted in both IMF2 and IMF3, but the effect is poor compared to the proposed method.

In this experimental analysis, FCFs are successfully extracted from the component envelope spectra obtained by SGMD and EMD decomposition. However, when compared with the envelope spectra of the proposed methods, it is clear that they suffer from a certain degree of interference from noisy spectral lines.

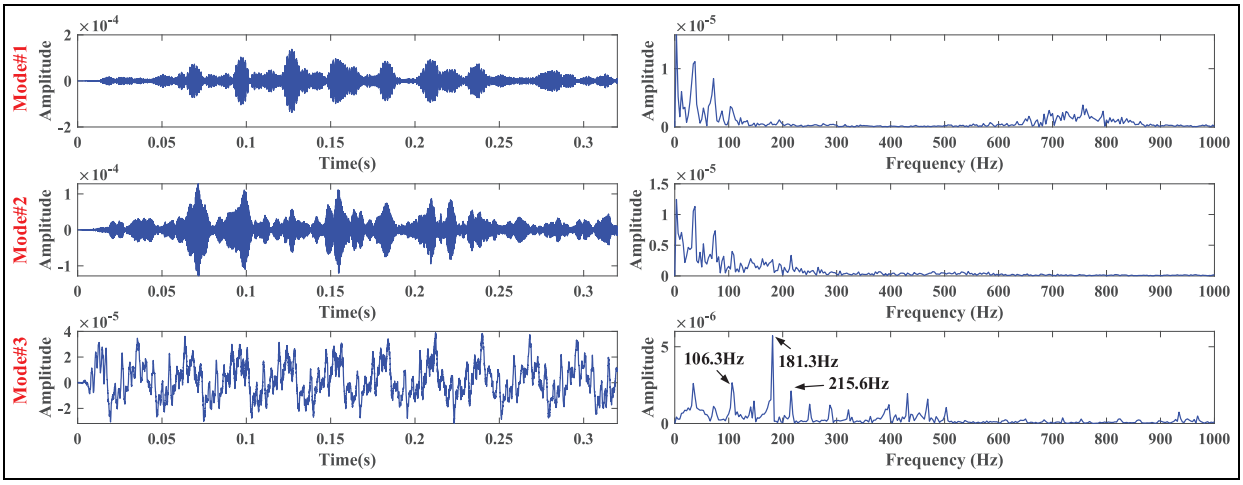

Figure 34. Decomposition result of FMD with $n = 3$ for the bearing signal with an outer race fault.
FMD: Feature mode decomposition.

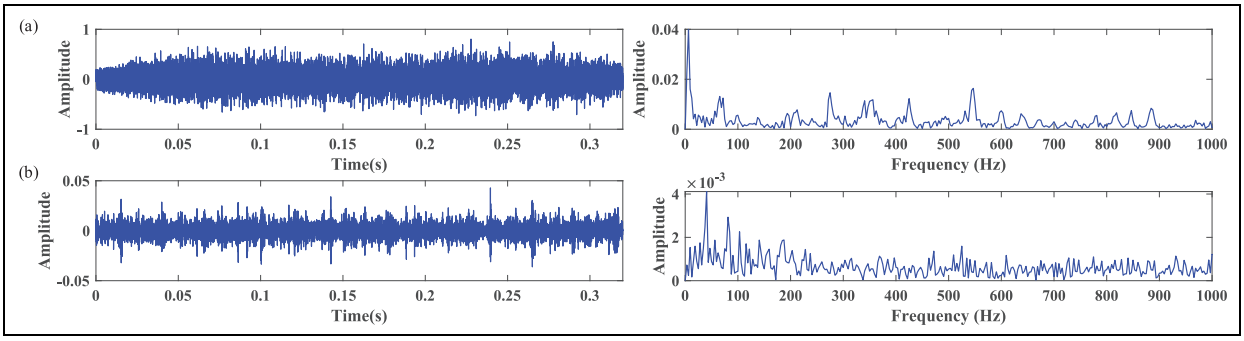

Figure 35. SRMD and SGMD deal with the bearing signal with an outer race fault: (a) SRMD and (b) SGMD.
SGMD: Symplectic geometric mode decomposition; SRMD: Sparse random mode decomposition.

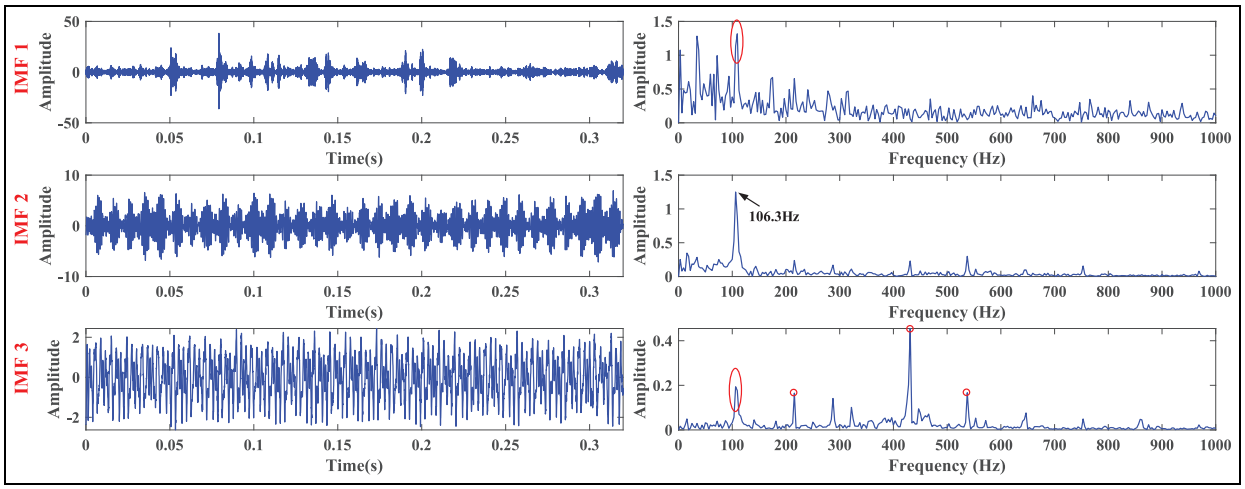

Figure 36. First three components of the VMD result for the bearing signal with an outer race fault.
VMD: Variational mode decomposition.

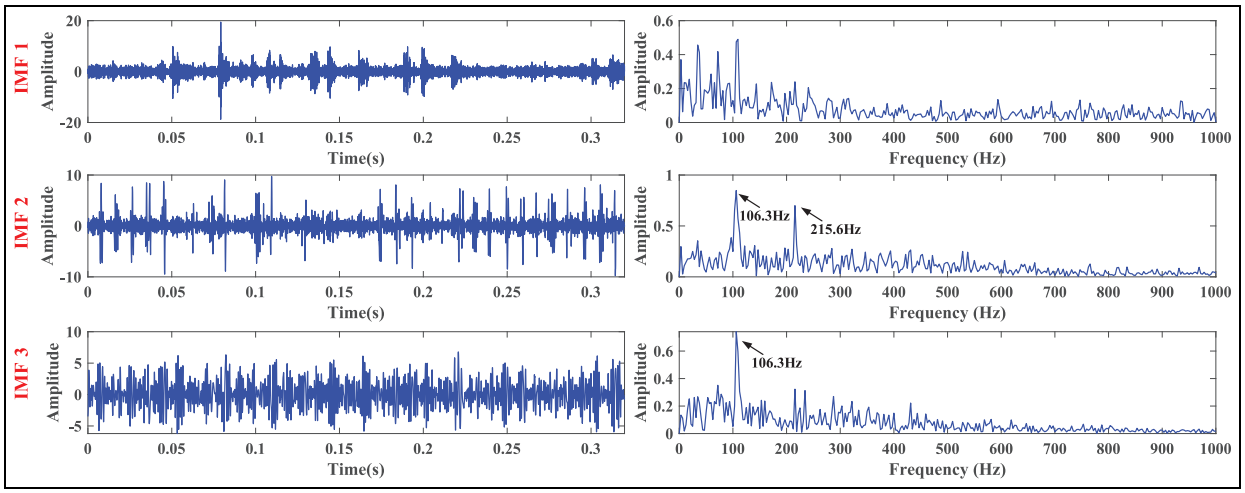

Figure 37. First three components of the EMD result for the bearing signal with an outer race fault.
EMD: Empirical mode decomposition.

Moreover, FMD, SRMD, and VMD are not found to be powerful enough for bearing fault diagnosis.

Conclusion

In order to solve the problem of setting the optimal FMD parameters, a new parameter estimation method is proposed to realize the FMD adaptively by using the relationship between faulty and healthy signals. It is also combined with spectral subtraction to highlight the fault characteristics within the signal. They are then fully decomposed using the improved FMD to select the effective fault components, which avoid the redundancy of fault signals or the omission of crucial fault information. Finally, the fault components are identified from the decomposed signals through Hilbert envelope spectral analysis. Through experimental analyses of single and compound faults in rotating machinery bearings, along with simulation studies and publicly dataset, the necessity and effectiveness of the proposed method are thoroughly validated. The proposed method's application performance and stability are further confirmed by processing engineering data. The proposed method demonstrates greater effectiveness in detecting faults in rotating machinery when compared to the five current techniques.

Future research will focus on optimizing the adaptive FMD method to perform stably under variable operating conditions (e.g. changing speeds and loads) of rotating machinery, enhancing its adaptability in

practical industrial environments. Additionally, efforts will be made to extend this method to fault diagnosis of other key components (such as gears) and explore its effectiveness in multifault coupling scenarios. Furthermore, integrating it with lightweight intelligent algorithms to achieve real-time fault detection will be a priority, aiming to provide more efficient technical support for equipment health monitoring.

Declaration of conflicting interests

The authors declared no potential conflicts of interest with respect to the research, authorship, and/or publication of this article.

Funding

The authors disclosed receipt of the following financial support for the research, authorship, and/or publication of this article: The authors are grateful for the support of the National Natural Science Foundation of China (No. 52375116), the Wenzhou Major Science and Technology Innovation Project of China (No. ZG2023029), the Wenzhou Municipal Science and Technology Bureau, China (No. G20240042).

ORCID iDs

Yi Liu https://orcid.org/0009-0004-3346-6082
Jiawei Xiang https://orcid.org/0000-0003-4028-985X

References

1. Heng A, Zhang S, Tan A CC, et al. Rotating machinery prognostics: state of the art, challenges and opportunities. *Mech Syst Signal Pr* 2009; 23(3): 724–739.
2. Liang PF, Yu ZZ, Wang B, et al. Fault transfer diagnosis of rolling bearings across multiple working conditions via subdomain adaptation and improved vision transformer network. *Adv Eng Inform* 2023; 57: 102075.
3. Chen ZX, He CB, Liu Y B, et al. Incipient fault feature extraction of rolling bearing based on optimized singular spectrum decomposition. *IEEE Sens J* 2021; 21(18): 20362–20374.
4. Wang B, Lei YG, LI NP, et al. A hybrid prognostics approach for estimating remaining useful life of rolling element bearings. *IEEE T Reliab* 2020; 69(1): 401–412.
5. Zhu HX, Jiang HK, Yao RH, et al. Rolling bearing incipient fault feature extraction using impulse-enhanced sparse time-frequency representation. *Meas Sci Technol* 2023; 34(10): 105124.
6. Wang ZY, Yao LG, Cai YW, et al. Mahalanobis semi-supervised mapping and beetle antennae search based support vector machine for wind turbine rolling bearings fault diagnosis. *Renew Energ* 2020; 155: 1312–1327.
7. Hou BC, Wang D, Xia TB, et al. Difference mode decomposition for adaptive signal decomposition. *Mech Syst Signal Pr* 2023; 191: 110203.
8. Wang YZ, Wu JH, Yu ZY, et al. A structurally re-parameterized convolution neural network-based method for gearbox fault diagnosis in edge computing scenarios. *Eng Appl Artif Intel* 2023; 126: 107091.
9. Guo JC, Liu Y, Yang RG, et al. Ensemble difference mode decomposition based on transmission path elimination technology for rotating machinery fault diagnosis. *Mech Syst Signal Pr* 2024; 212: 111330.
10. Shao HD, Zhou XD, Lin J, et al. Few-shot cross-domain fault diagnosis of bearing driven by Task-supervised ANIL. *IEEE Internet Things* 2024; 11(13): 22892–22902.
11. Zhao M and Jia XD. A novel strategy for signal denoising using reweighted SVD and its applications to weak fault feature enhancement of rotating machinery. *Mech Syst Signal Pr* 2017; 94: 129–147.
12. Yan S, Shao HD, Wang J, et al. LiConvFormer: a lightweight fault diagnosis framework using separable multiscale convolution and broadcast self-attention. *Expert Syst Appl* 2024; 237: 121338.
13. Han CK, Lu W, Cui LL, et al. Improved shift-invariant sparse parsing of mechanical fault based on feature atom. *IEEE T Instrum Meast* 2024; 73: 6504412.
14. Guo JC, Liu Y, Li JH, et al. Rotating machinery fault detection using a new version of intrinsic time-scale decomposition. *IEEE Sens J* 2023; 24(2): 1905–1918.
15. Lu JT, Jia B, Li SM, et al. A noise reduction method of rolling bearing based on empirical wavelet transform and adaptive time frequency peak filtering. *Meas Sci Technol* 2023; 34(12): 125146.
16. Ge Y, Zhang FS and Ren Y. Adaptive fault diagnosis method for rotating machinery with unknown faults under multiple working conditions. *J Manuf Syst* 2022; 63: 177–184.
17. Li Y, Chen G, Mas SC, et al. Bearing fault diagnosis method based on complete center frequency distribution feature. *Struct Health Monit* 2023; 22(6): 4100–4116.
18. Zhou J, Yang Y, Wang P, et al. Multivariate local fluctuation mode decomposition and its application to gear fault diagnosis. *Measurement* 2023; 214: 112769.
19. Liu F, Cheng JS, Hu NQ, et al. A novel random spectral similar component decomposition method and its application to gear fault diagnosis. *Mech Syst Signal Pr* 2023; 208: 111032.
20. Liu JY, Xie FQ, Zhang Q, et al. A multisensory time-frequency features fusion method for rotating machinery fault diagnosis under nonstationary case. *J Intell Manuf* 2023; 35(7): 3197–3217.
21. Jin H, Lin JH, Chen XQ, et al. Modal parameters identification method based on symplectic geometry model decomposition. *Shock Vib* 2019; 2019: 5018732.
22. Gu J, Peng YX, Lu H, et al. An optimized variational mode decomposition method and its application in vibration signal analysis of bearings. *Struct Health Monit* 2022; 21(5): 2386–2407.
23. Miao YH, Zhang BY, Li CH, et al. Feature mode decomposition: new decomposition theory for rotating machinery fault diagnosis. *IEEE T Ind Electron* 2022; 70(2): 1949–1960.

24. Yan XA, Yan WJ, Xu YD, et al. Machinery multi-sensor fault diagnosis based on adaptive multivariate feature mode decomposition and multi-attention fusion residual convolutional neural network. *Mech Syst Signal Pr* 2023; 202: 110664.
25. Yan XA and Jia MP. Bearing fault diagnosis via a parameter-optimized feature mode decomposition. *Measurement* 2022; 203: 112016.
26. Li ZP, Zhou ZT and Zhou XY. A sensor-based modified FMD method to identify fault feature for mechanical fault diagnosis of ship-borne antennae. *IEEE Access* 2023; 11: 40018–40028.
27. Huang SX, Wang XP, Li CF, et al. Data decomposition method combining permutation entropy and spectral substitution with ensemble empirical mode decomposition. *Measurement* 2023; 139: 438–453.
28. Li H, Wang TY, Zhang FB, et al. FMDPgram: an improvement of FMD for rotating machinery fault diagnosis. *IEEE T Ind Inform* 2025; 21(8): 6398–6409.
29. He XZ, Zhou XQ, Li JL, et al. Adaptive feature mode decomposition: a fault-oriented vibration signal decomposition method for identification of multiple localized faults in rotating machinery. *Nonlinear Dynam* 2023; 111(17): 16237–16270.
30. Dai HZ, Li DS and Beer M. Adaptive Kriging-assisted multi-fidelity subset simulation for reliability analysis. *Comput Method Appl M* 2025; 436: 117705.
31. Gu JX, Wang ZH, Kuen J, et al. Recent advances in convolutional neural networks. *Pattern Recongn* 2018; 77: 354–377.
32. Ibrahim R and Shafiq MO. Explainable convolutional neural networks: A taxonomy, review, and future directions. *Acm Comput Surv* 2023; 55(10): 206.
33. Richardson N, Schaeffer H and Tran G. SRMD: Sparse random mode decomposition. *Com Appl Math Comput* 2024; 6(2): 879–906.
34. Guo JC, Liu Y, Yang RG, et al. Differgram: A convex optimization-based method for extracting optimal frequency band for fault diagnosis of rotating machinery. *Expert Syst Appl* 2024; 245: 123051.
35. Chen XW and Feng ZP. Order spectrum analysis enhanced by surrogate test and Vold-Kalman filtering for rotating machinery fault diagnosis under time-varying speed conditions. *Mech Syst Signal Pr* 2021; 154: 107585.
36. Tang M, Liao YX, Luo F, et al. A Novel Method for Fault Diagnosis of Rotating Machinery. *Entropy-switz* 2022; 24(5): 681.
37. Yin N, Meng Z, Guan Y, et al. An adaptive multiple time domain synchronous averaging method and its application in vibration signal feature enhancement. *Meas Sci Technol* 2022; 33(5): 055004.
38. Liu ZL, Peng DD, Zuo MJ, et al. Improved Hilbert-Huang transform with soft sifting stopping criterion and its application to fault diagnosis of wheelset bearings. *ISA T* 2022; 125: 426–444.
39. Cheng J, Yang Y, Wu ZT, et al. Fault diagnosis ramanujan fourier mode decomposition and its application in gear. *IEEE T Ind Inform* 2022; 18(9): 6079–6088.
40. Liu H and Xiang JW. Kernel regression residual decomposition-based synchroextracting transform to detect faults in mechanical systems. *ISA T* 2019; 87: 251–26.
41. Meng LJ, Xiang JW, Wang YX, et al. A hybrid fault diagnosis method using morphological filter-translation invariant wavelet and improved ensemble empirical mode decomposition. *Mech Syst Signal Pr* 2015; 50: 101–115.